STM JOURNALS

Journal of
Offshore Structure and Technology

ISSN: 2349-8986
Volume 11, Issue 3, 2024
September–December
DOI (Journal): 10.37591/JoOST

https://journals.stmjournals.com/joost

Research JoOST

Analysis of the Output Power in Offshore Bladeless Vibrational Wind Turbines

Ignacio Madrazo[1,*], Carlos Armenta-Déu[2], Jorge Contreras[2], Matilde Santos[3]

Abstract

This work focuses on studying and analyzing the power generation in offshore bladeless vibrational wind turbines. In previous work, we developed detailed research about the vibrational wind turbine design and configuration; in this new work, we analyze the energy supply from this type of turbine to achieve a better understanding of the behavior and potential of bladeless vibrational wind turbines (BVWT) as an additional power source in offshore wind farms. This paper evaluates the BVWT power coefficient to determine the turbine performance. The study also analyzes the factors influencing wind turbine behavior and how changing these parameters can improve turbine efficiency. The simulation results prove that BVWT represents a feasible and reliable power source in wind farms, with the wind turbines operating at optimum conditions in turbulent winds.

Keywords: Wind energy, bladeless vibrational wind turbine, performance simulation and optimization, turbulent wind regime operation, output power, energy generation

INTRODUCTION

The development of offshore wind farms as an alternative to inland facilities represents a challenge in generating maximum available power. To this end, increasingly powerful turbines are being installed on the seabed in various parts of the world [1]. Offshore wind turbines often benefit from a stable and regular wind flow in a laminar regime. Nevertheless, the turbulence generated by a wind turbine forces adjacent turbines to separate the minimum distance to avoid wake effects [2–7]. Because the offshore wind farm layout requires specific separation between the next turbines, both in the wind direction and crosswise, the offshore wind farm power density has a limit, which increases if we use the free space between turbines to place smaller wind turbines operating in turbulent wind conditions. A similar situation is generated by wake effects.

***Author for Correspondence**
Ignacio Madrazo
E-mail: masterenergyucm@gmail.com

[1]PG Student, Department of Matter Structure, Thermal Physics and Electronics, Faculty of Physical Sciences, Complutense University of Madrid, 28040 Madrid, Spain
[2]Professor, Department of Matter Structure, Thermal Physics and Electronics, Faculty of Physical Sciences, Complutense University of Madrid, 28040 Madrid, Spain
[3]Professor, Department of Computer Architecture and Automatic Control, Faculty of Computer Science, Complutense University of Madrid, 28040 Madrid, Spain

Received Date: October 07, 2024
Accepted Date: October 09, 2024
Published Date: October 10, 2024

Citation: Ignacio Madrazo, Carlos Armenta-Déu, Jorge Contreras, Matilde Santos. Analysis of the Output Power in Offshore Bladeless Vibrational Wind Turbines. Journal of Offshore Structure and Technology. 2024; 11(3): 12–23p.

Conventional three-blade horizontal-axis wind turbines are not suitable for turbulent winds, reducing efficiency [8–10], increasing fatigue and wear [11, 12], and provoking damage [13]. Although vertical axis wind turbines are less prone to damage under turbulent winds, they continue to experience fatigue and wear when operating under turbulent wind regimes [14, 15]. Recently, some researchers have suggested intercalating small three-blade horizontal-axis wind turbines specifically designed to operate under drag force, which are compatible with turbulent winds [16, 17]. Another possibility for using turbulent winds as the primary force is the use of bladeless turbines, which use the vortex effect to vibrate the wind turbine and generate electric energy [18–22].

Bladeless turbines are characterized by a symmetric design that allows the reception of wind from any direction without affecting the force distribution on the turbine structure [23, 24]. These characteristics make bladeless turbines suitable for areas where turbulent winds or wakes are present if they operate in vibrational mode [25, 26]. Bladeless turbines currently operate onshore because of their simple design, low cost, and ease of installation [27, 28]; however, they are also suitable for offshore applications, either anchored to the seabed or floating because of their symmetric design [23, 29, 30].

In this work, we study and analyze a new model of a bladeless wind turbine operating in vibrational mode for installation in offshore wind farms as a solution to increase the output power without altering the existing layout. This study characterizes bladeless wind turbine performance and evaluates its output power as the most relevant parameter.

THEORETICAL FOUNDATIONS

We consider a bladeless vibrational wind turbine as a mechanical system that oscillates around the vertical axis of symmetry, as shown in Figure 1. The analysis of oscillatory movement considers the bladeless turbine as a group of narrow solid disks of mass *mi* linked to a wall through an elastic spring following Hook's law. The mechanical energy of a bladeless turbine is the sum of the energy associated with each disk or segment.

Applying the Mechanic laws for an oscillatory movement, we have:

$$\xi_{mech,i} = \frac{1}{2} k x_i^2 \tag{1}$$

ξ is the mechanical energy of the disk, *i* and *k* are the bladeless turbine material elastic constants, and *x* is the horizontal displacement from the vertical axis of segment *i*.

Equation (1) can be rewritten as a function of angular frequency ω as follows:

$$\xi_{mech,i} = \frac{1}{2} m_i \omega^2 x_i^2 \tag{2}$$

Considering an elemental disk of infinitesimal thickness, Equation (2) adopts the form:

$$d\xi_{mech,i} = \frac{1}{2} \rho \omega^2 x_i^2 dV_i \tag{3}$$

ρ is the turbine material density and *dV* is the disk differential volume, which depends on the solidity of the material.

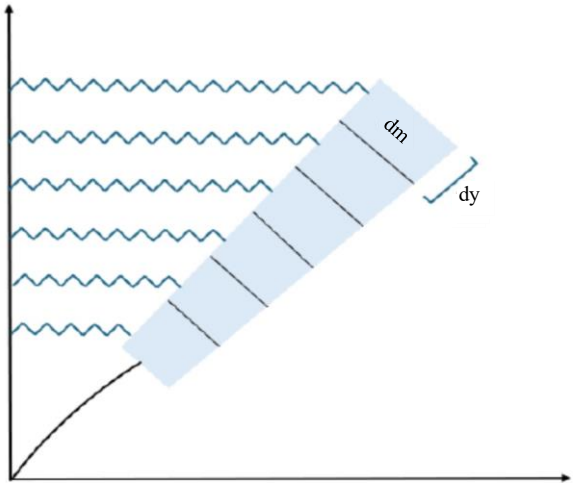

Figure 1. Schematic representation of the oscillation mode for the bladeless vibrational wind turbine.

For a simpler solution, we consider the turbine to be a solid material; therefore, the differential volume is

$$dV_i = S_{tr,i} dy_i = \frac{\pi}{4} D_i^2 dy_i \tag{4}$$

D is the diameter of the disk and *y* is the relative height of the turbine base.

Combining Equations (3) and (4) and expressing the mechanical energy as a function of the oscillation frequency *f*, we have

$$d\xi_{mech,i} = \frac{\pi^3}{2} \rho f^2 x_i^2 D_i^2 dy_i \tag{5}$$

The solution of Equation (5) requires defining *x* and *D* in terms of *y*. If we retrieve these expressions from a previous study [31],

$$x_i = \left(\frac{y_i - L/2}{H - L/2}\right) \beta D_i \tag{6}$$

$$D_i = \left\{ \frac{d_i^2}{V_{i=L/2}^2} \left[V_i^2 + \frac{16 S_i t^2 \beta^2 V_{i=L/2}^2}{1 - 16 S_i t^2 \beta^2} \left(\frac{y_i - L/2}{H - L/2}\right) \right] \right\}^{1/2} \tag{7}$$

with

$$\beta = (x_{i=L} / D_{i=L}) \tag{8}$$

Now, replacing in Equation (5):

$$d\xi_{mech,i} = \frac{\pi^3}{2} \rho f^2 \left[\left(\frac{y_i - L/2}{H - L/2}\right) \beta D_i \right]^2 \left[\frac{d_i^2}{V_{i=L/2}^2} \left[V_i^2 + \frac{16 S_i t^2 \beta_{ds}^2 V_{i=L/2}^2}{1 - 16 S_i t^2 \beta_{ds}^2} \left(\frac{y_i - L/2}{H - L/2}\right) \right] \right] dy_i \tag{9}$$

It is important to note that we used two values, *b*, to characterize the oscillation amplitude and *bds* for the bladeless wind turbine design, respectively. At the moment of turbine design, we impose *bds*=1, which automatically defines the material density because both parameters are related to each other through the following expression:

$$\rho = \frac{1}{\beta^2} \tag{10}$$

Nevertheless, *b* cannot depend only on aerodynamics because two turbine masts built aerodynamically identical, but in different materials, would have the same oscillation frequency, which is false. If a single *b* appears in Equation (9), the energy may rise to infinity, which is physically impossible.

The method to compensate for the density dependence is a variation in the maximum oscillation; looking at Equation (8), we notice that all terms are above zero and constant. If we normalize to 1 to analyze the relationship between *b* and *r*, we obtain Equation (10). In Figure 2, we observe that density dependence on *b* follows the expected trend; if the turbine mast oscillates at a high amplitude, the density should be low, and vice versa. This statement is consistent with the physical fact that a heavy mast oscillates at a low amplitude, whereas a light mast has high oscillations.

Solving Equation (9):

$$\xi = A \int_{L/2}^{H} \left(\frac{y_i - L/2}{H - L/2}\right)^2 V_i^2 dy_i + AB \int_{L/2}^{H} \left(\frac{y_i - L/2}{H - L/2}\right)^4 dy_i = AI_2 + ABI_1 \tag{11}$$

With:

$$A = \frac{\pi^3}{2} \rho f^2 \beta^2 D_H^2 \frac{d^2}{V_{L/2}^2} \tag{12}$$

$$B = \frac{16 S t^2 \beta_{ds}^2 V_H^2}{1 - 16 S t^2 \beta_{ds}^2} \tag{13}$$

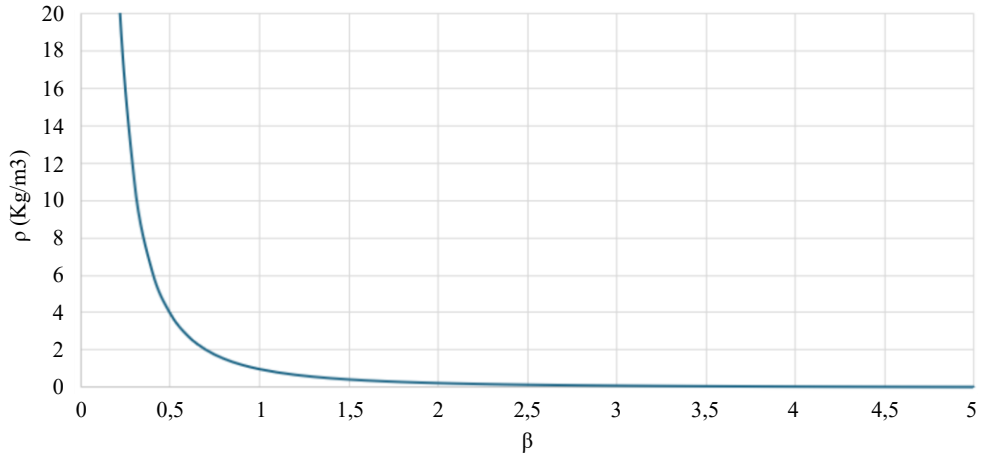

Figure 2. Density evolution with β.

The solution for integrals I_1 and I_2 is:

$$I_1 = \int_{y_i=L/2}^{y_i=H} \left(\frac{y_i - L/2}{H - L/2}\right)^4 dy_i = \int_0^1 t^4 \left(H - \frac{L}{2}\right) dt = \frac{1}{5}\left(H - \frac{L}{2}\right) \; with \; t = \frac{y_i - L/2}{H - L/2} \rightarrow dt = \frac{dy_i}{H - L/2} \tag{14}$$

and

$$\begin{aligned} I_2 = \int_{y_i=L/2}^{y_i=H} \left(\frac{y_i - L/2}{H - L/2}\right)^2 V_i^2 dy_i &= \int_{y_i=L/2}^{y_i=H} \left(\frac{y_i - L/2}{H - L/2}\right)^2 \frac{V_{ref}^2}{y_{ref}^{2\alpha}} y_i^{2\alpha} dy_i \\ &= C \int_{y_i=L/2}^{y_i=H} (y_i - L/2)^2 \, y_i^{2\alpha} dy_i = C \int_{y_i=L/2}^{y_i=H} \left(y_i^2 - L y_i + \frac{L^2}{4}\right) y_i^{2\alpha} dy_i \\ &= C \left[\frac{H^{2\alpha+3}}{2\alpha+3} - \frac{L^{2\alpha+3}}{(16\alpha+24)2^{2\alpha}} - L\left(\frac{H^{2\alpha+2}}{2\alpha+2} - \frac{L^{2\alpha+2}}{(8\alpha+8)2^{2\alpha}}\right)\right. \\ &\left. + \frac{L^2}{4}\left(\frac{H^{2\alpha+1}}{2\alpha+1} - \frac{L^{2\alpha+1}}{(4\alpha+2)2^{2\alpha}}\right)\right] \text{with } C = \left(\frac{V_{ref}^2}{(H - L/2)^2}\right)^2 y_{ref}^{2\alpha} \end{aligned} \tag{15}$$

Replacing in Equation (11):

$$\begin{aligned} \xi = \frac{\pi^3}{2} \rho f^2 \beta^2 D_H^2 \frac{d^2}{V_{L/2}^2} \left[\frac{V_{ref}^2}{(H - L/2)^2 \, y_{ref}^{2\alpha}} \left[\frac{H^{2\alpha+3}}{2\alpha+3} - \frac{L^{2\alpha+3}}{(16\alpha+24)2^{2\alpha}} - L\left(\frac{H^{2\alpha+2}}{2\alpha+2} - \frac{L^{2\alpha+2}}{(8\alpha+8)2^{2\alpha}}\right)\right.\right. \\ \left.\left. + \frac{L^2}{4}\left(\frac{H^{2\alpha+1}}{2\alpha+1} - \frac{L^{2\alpha+1}}{(4\alpha+2)2^{2\alpha}}\right)\right] + \frac{16 St^2 \beta_{ds}^2 V_H^2}{1 - 16 St^2 \beta_{ds}^2} \left(\frac{H - L/2}{5}\right)\right] \end{aligned} \tag{16}$$

WIND POWER

This section describes the wind power calculation for the bladeless wind turbine mast. Using the classical expression [32],

$$P_w = \frac{1}{2} \rho_{air} S u^3 \tag{17}$$

Because wind speed changes with height, the following equation applies [33]:

$$u_y = u_{ref} \left(\frac{y}{y_{ref}}\right)^{\alpha} \tag{18}$$

In addition, the wind strikes the front cross-section of the wind turbine; therefore, Equation (17) should be rewritten in differential form as follows:

$$dP_w = \frac{1}{2}\rho_{air} D_y u_y^3 dy \tag{19}$$

The parameter *y* indicated the disk or segment height.

If we integrate over the entire mast length:

$$P_w = \frac{1}{2}\rho_{air}\int_{L/2}^{H} D_y u_y^3 dy = \frac{1}{2}\rho_{air}\frac{d}{u_{L/2}}\int_{L/2}^{H}\left[\mu_i^2 + \frac{16St^2\beta_{ds}^2 V_H^2}{1-16St^2\beta_{ds}^2}\left(\frac{y-L/2}{H-L/2}\right)\right]^{1/2} u_y^3 dy \tag{20}$$

Because the analytical solution of Equation (20) is complex, we apply a linear approximation [31]. Therefore,

$$D_y = a + by \tag{21}$$

With:

$$a = d - \frac{D_H - Ld}{H-L/2};\ b = \frac{D_H - d}{H-L/2} \tag{22}$$

Combining Equations (20), (21) and (22):

$$\begin{aligned} P_w &= \frac{1}{2}\rho_{air}\left[\int_{L/2}^{H} a\frac{u_{ref}^3}{y_{ref}^{3\alpha}} y^{3\alpha} dy + \int_{L/2}^{H} b\frac{u_{ref}^3}{y_{ref}^{3\alpha}} y^{3\alpha+1} dy\right] \\ &= \frac{1}{2}\rho_{air}\frac{u_{ref}^3}{y_{ref}^{3\alpha}}\left[a\int_{L/2}^{H} y^{3\alpha} dy + b\int_{L/2}^{H} y^{3\alpha+1} dy\right] \\ &= \frac{1}{2}\rho_{air}\frac{u_{ref}^3}{y_{ref}^{3\alpha}}\left[a\left(\frac{H^{3\alpha+1}}{3\alpha+1} - \frac{L^{3\alpha+1}}{(6\alpha+2)2^{3\alpha}}\right) + b\left(\frac{H^{3\alpha+2}}{3\alpha+2} - \frac{L^{3\alpha+2}}{(12\alpha+8)2^{3\alpha}}\right)\right] \\ &= \frac{1}{2}\rho_{air}\frac{u_{ref}^3}{y_{ref}^{3\alpha}}\left[\left(d - \frac{D_H - d}{H-L/2}\frac{L}{2}\right)\left(\frac{H^{3\alpha+1}}{3\alpha+1} - \frac{L^{3\alpha+1}}{(6\alpha+2)2^{3\alpha}}\right)\right. \\ &\quad \left. + \left(\frac{D_H - d}{H-L/2}\right)\left(\frac{H^{3\alpha+2}}{3\alpha+2} - \frac{L^{3\alpha+2}}{(12\alpha+8)2^{3\alpha}}\right)\right] \end{aligned} \tag{23}$$

Power Coefficient

The power coefficient is defined as the mechanic-to-wind energy ratio. Converting mechanical power into energy yields:

$$P_{mech} = 2\xi_{mech} f \tag{24}$$

Therefore, the power coefficient is:

$$C_P = \frac{2\xi_{mech} f}{P_w} \tag{25}$$

Because the mechanical power depends either on the material density, ρ, or the coefficient β, and because ρ and β depend on each other, Equation (25) represents a linear function with two independent variables: the power coefficient and the material density or the β-coefficient. Therefore, we developed an iterative process to determine the power coefficient, which validates Equation (25).

To this end, we applied a Python program to simulate the mathematical functions for mechanical and wind power using the following operating and design specifications:

$$d = D_{L/2};\ f = f\left(\frac{L}{2}\right);\ u_y = u_{ref}\left(\frac{y}{y_{ref}}\right)^{\alpha};\ u_{osc} = 4x_y f$$
$$\beta = \frac{x_H}{D_H};\ x_y = x_H\left(\frac{y - L/2}{H - L/2}\right) \tag{26}$$

Power Coefficient Dependence on Turbine Mast Height

The first step of the simulation is calculating the wind and mechanical power using Equations (16) and 23, considering all parameters constant except the turbine mast height, which varies from 0 to 10 m. Figure 3 shows the wind and mechanical power evolution with turbine mast height.

Repeating the process for efficiency (Figure 4) yields. It should be noted that the efficiency data in Figure 4 are not accurate because we used arbitrary values for ρ and β. Nevertheless, we observe that efficiency evolution is coherent with the current values in a wind turbine [34], showing a peak value of approximately 59%, which matches the maximum attainable according to Betz's law [35]. Therefore, we can validate the proposed mathematical model for the power and efficiency evolution with turbine mast height.

Because the simulation considers a turbine core 2 m high, values for mast heights below 2 m (dashed red line in Figure 4) are inconsistent; therefore, we only use mast heights above 2 m, where the efficiency decays continuously. We conclude that the bladeless turbine efficiency decreases with an increase in the mast height.

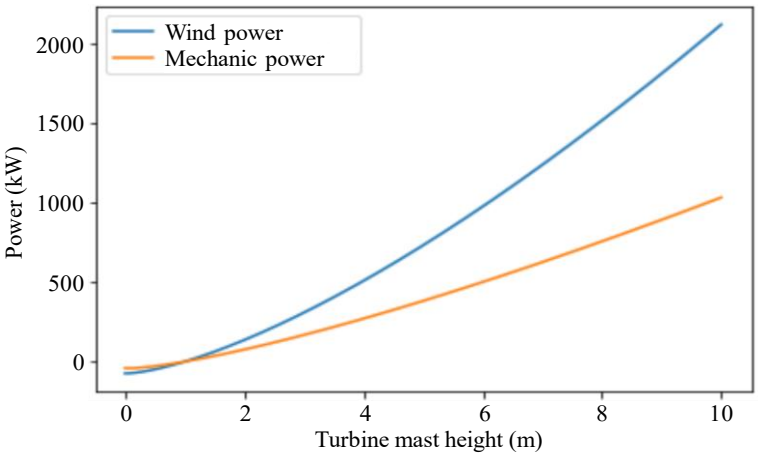

Figure 3. Wind and mechanic power evolution with turbine mast height.

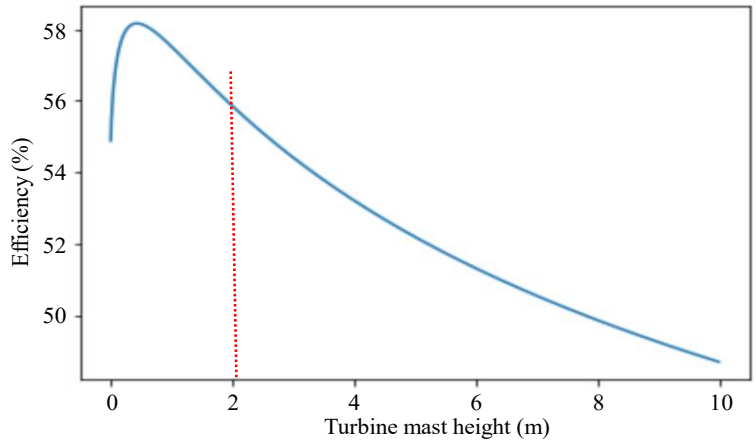

Figure 4. Efficiency evolution with turbine mast height.

Power Coefficient Dependence on Turbine Core Height

We repeated the process by changing the turbine core height and maintaining all the other parameters constant. We changed the core height from 0 to 2 m. Figure 5 shows the simulation results for wind and mechanical power, while Figure 6 shows the efficiency.

Efficiency continuously decreases with the height of the core. This conclusion is consistent with the claim that a higher core increases the mast height and reduces turbine efficiency. The continuous decrease in efficiency is also consistent with the current evolution of turbine efficiency, proving the validity of the proposed methodology. Therefore, we conclude that it is impossible to increase turbine power generation unlimitedly by increasing the height of the core or mast.

Power Coefficient Dependence on Terrain Rugosity Coefficient

The third simulation process aimed to evaluate the power coefficient evolution with terrain rugosity variations. We applied a rugosity coefficient variation between 0 and 0.4, as this is the matching interval to the Earth's surface rugosity variation. Figure 7 shows the mechanical and wind power evolution with terrain rugosity variations. Figure 8 shows the evolution of efficiency.

We notice that efficiency increases with terrain rugosity, consistent with bladeless wind turbines, specifically designed to operate in turbulent winds, a typical situation on rough terrain. The linear efficiency dependence on terrain rugosity may lead to the conclusion that the efficiency may reach values above 100%, which is inconsistent. Nevertheless, because we constrained the α-value to the interval 0-0.4, according to the simulation, the efficiency never exceeded 70%.

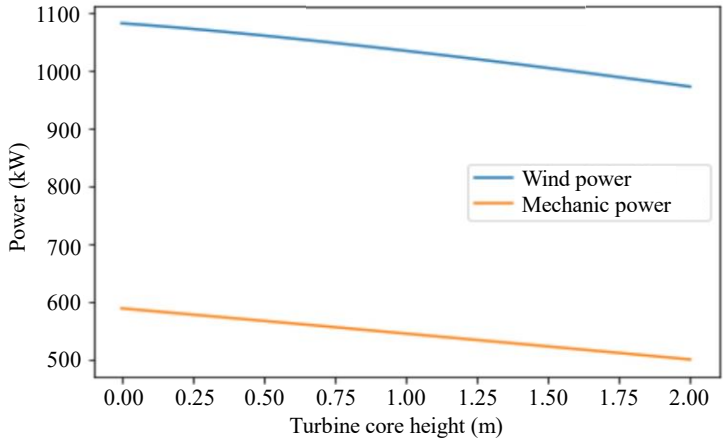

Figure 5. Wind and mechanic power evolution with turbine core height.

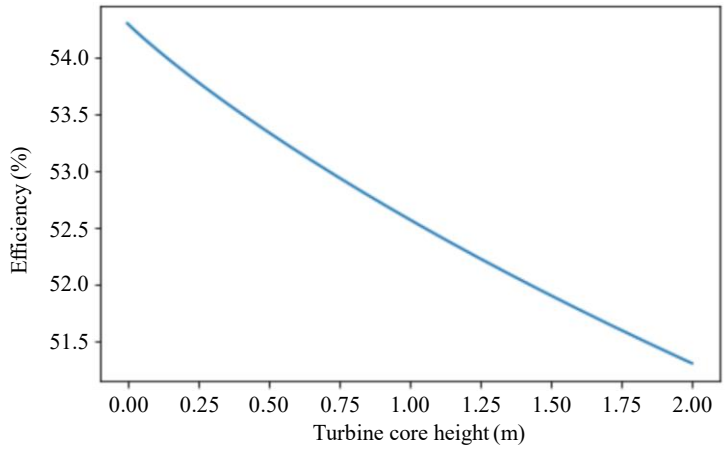

Figure 6. Efficiency evolution with turbine core height.

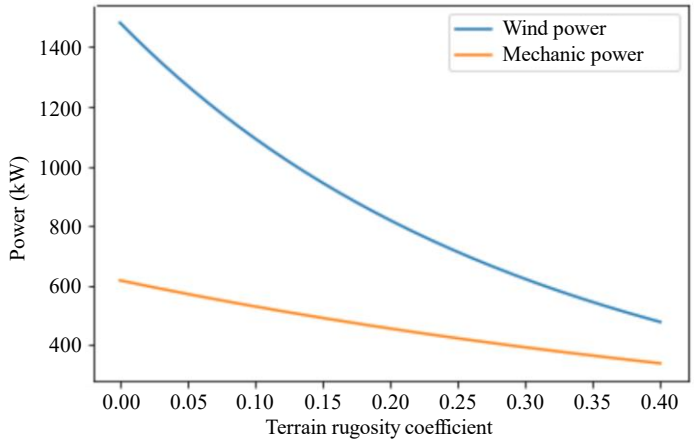

Figure 7. Wind and mechanic power evolution with terrain rugosity coefficient.

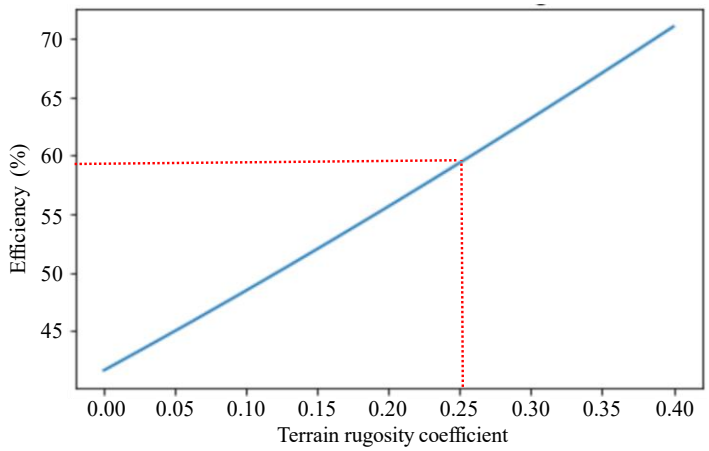

Figure 8. Efficiency evolution with terrain rugosity coefficient.

On the other hand, it looks like efficiency values for terrain rugosity coefficient above 0.25 are inconsistent because the efficiency exceeds the theoretical limit of 59% established by Betz's law [35]; however, this statement is incorrect because we are operating in turbulent wind where Betz's law does not apply.

Power Coefficient Dependence on Wind Reference Speed

We repeated the simulation process, modifying the wind reference speed, and obtained the following results (Figures 9 and 10): Once again, the efficiency evolution is consistent with the expected results because of the turbine operation in turbulent winds.

Power Coefficient Dependence on Turbine Mast Diameter and Vortex Generation

This simulation process deals with the dependence on turbine mast diameter and vortex generation. This analysis is relevant because the turbine diameter at the lowest section, d, determines the diameter at the highest point; thus, the turbine geometrical shape and oscillation frequency f, from which the power generation is derived [36]. Figures 11 and 12 show the power and efficiency evolutions for the lowest section turbine diameter.

The efficiency remained constant when the three parameters were applied together. This result is consistent because it proves that turbine efficiency does not increase without limits. In addition, the simulation demonstrates that there is no optimum value for the lowest section turbine diameter that maximizes the wind-to-mechanical power conversion; therefore, the diameter selection is a purely structural decision, depending on the turbine size.

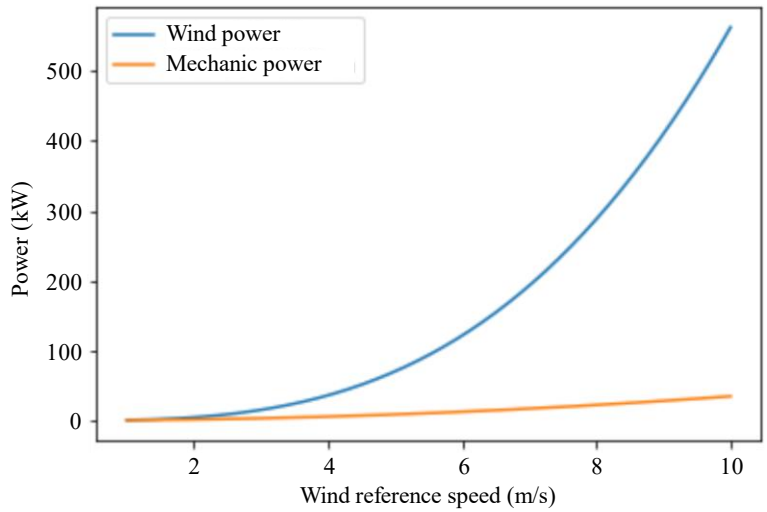

Figure 9. Wind and mechanic power evolution with wind reference speed.

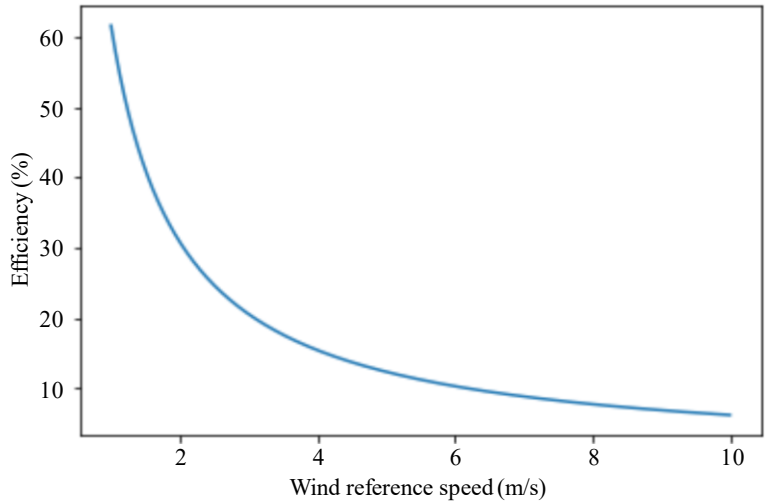

Figure 10. Efficiency evolution with wind reference speed.

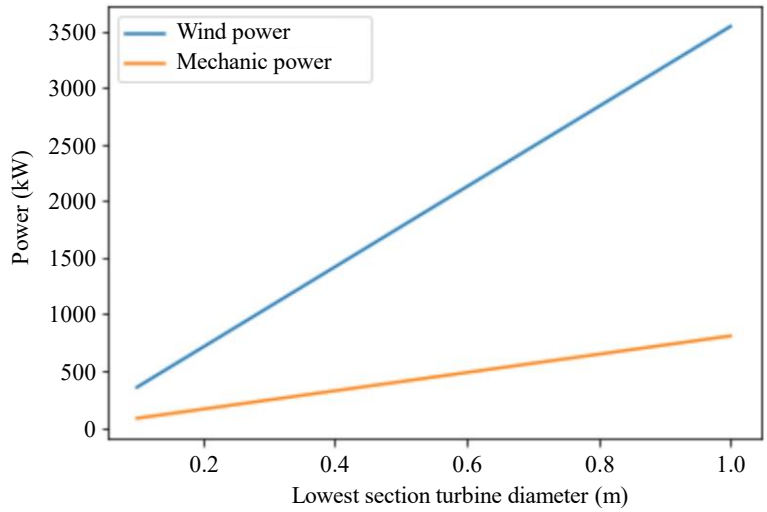

Figure 11. Wind and mechanic power evolution with lowest section turbine diameter.

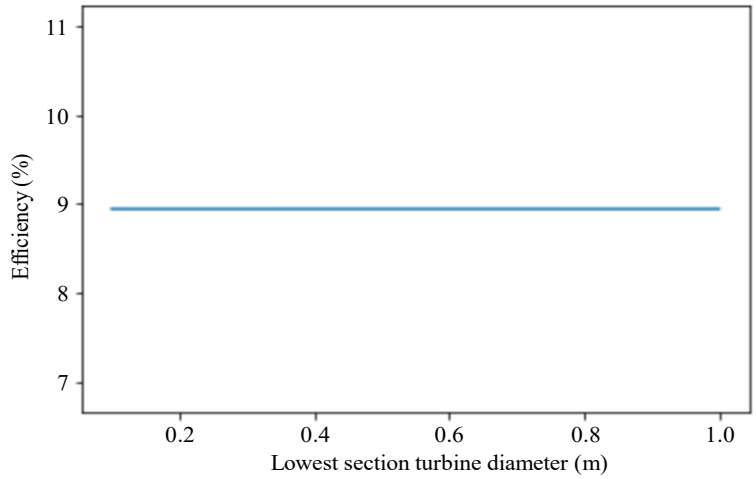

Figure 12. Efficiency evolution with lowest section turbine diameter.

Table 1. Coefficients for the linear dependence turbine efficiency on material density.

	β		
Coeff.	0.02	0.05	0.10
δ	0.0037	0.0012	0.0002
R^2	1.0		

δ is the linear regression slope.

Power Coefficient Dependence on Material Density

The last simulation analyzed the dependence of the power coefficient on the turbine material density. We simulated a constant β using three different options: β=0.02, β=0.05, and β=0.1. Once β is set up, only one variable remains because the other two parameters intervene in the calculation; the power coefficient and the material density, depend on each other. We constrain the analysis to an efficiency interval from 0 to 0.5, because this is the maximum attainable value under the current operating conditions.

The simulation showed a linear dependence between turbine efficiency and material density. Table 1 shows the linear regression coefficients of the analyzed cases. The data analysis from Table 1 shows that efficiency increases faster as the β-coefficient decreases, meaning that dense material provokes slower oscillations. Because the wind turbine mast is hollow, the specific material density is lower; therefore, the turbine oscillates more widely and faster, generating higher energy.

CONCLUSIONS

We have developed a detailed study of bladeless wind turbine efficiency as a function of various parameters, such as the turbine mast height and diameter, turbine core height, terrain rugosity, wind reference speed, and material density. For the design parameters, that is, mast or core height and lower or upper diameter, the power coefficient does not diverge, suggesting that the model appears correct because increasing the design parameters cannot generate infinite energy. As for the operating parameters, such as the roughness coefficient or the reference speed, we conclude that the model delivers a higher power coefficient when these variables take values associated with the turbulent regime for which, in theory, we design these turbines to work. In addition, because the oscillation frequency depends only on the aerodynamic profile, the oscillation amplitude can be adjusted based on the material density.

Based on the simulation results, BWTs are wind turbines with higher efficiencies at distances close to the ground, owing to the effects of roughness. For this reason, they could play an important role in replacing small VAWTs used in urban environments for self-consumption.

Regarding the positioning strategy between conventional wind turbines, and because the ground roughness effect at hub heights is negligible, a more exhaustive study is necessary with the predominant turbulent current modeled as the wake of the wind turbines to reach a more definitive conclusion.

REFERENCES

1. Wikipedia. (2024). List of offshore wind farms. [Online]. Wikipedia. Available from: https://en.wikipedia.org/wiki/List_of_offshore_wind_farms
2. Christiansen MB, Hasager CB. Wake effects of large offshore wind farms identified from satellite SAR. Remote Sens Environ. 2005;98:251–8. DOI: 10.1016/j.rse.2005.07.009.
3. González JS, Payán MB, Santos JR. Optimum wind turbines operation for minimizing wake effect losses in offshore wind farms. 2013 13th International Conference on Environment and Electrical Engineering (EEEIC), Wroclaw, Poland, 2013, pp. 188–92. DOI: 10.1109/EEEIC-2.2013.6737905.
4. Moskalenko N, Rudion K, Orths A. Study of wake effects for offshore wind farm planning. 2010 Modern Electric Power Systems, Wroclaw, Poland, 2010, pp. 1-7.
5. Cao J, Qin Z, Gao X, Pu T, Zhu W, Ke S, et al. Study of aerodynamic performance and wake effects for offshore wind farm cluster. Ocean Eng. 2023;280:114639. DOI: 10.1016/j.oceaneng.2023.114639.
6. Iracheta Cortez RI, Dorrego JR. Analysis of the wake effect in the distribution of wind turbines. IEEE Lat Am Trans. 2020;18:668–76. DOI: 10.1109/TLA.2020.9082209.
7. Kinzel M, Araya DB, Dabiri JO. Turbulence in vertical axis wind turbine canopies. Phys Fluids. 2015;27. DOI: 10.1063/1.4935111.
8. Barthelmie RJ, Jensen LE. Evaluation of wind farm efficiency and wind turbine wakes at the Nysted offshore wind farm. Wind Energy. 2010;13:573–86. DOI: 10.1002/we.408.
9. Barthelmie RJ, Frandsen ST, Nielsen MN, Pryor SC, Rethore PE, Jørgensen HE. Modelling and measurements of power losses and turbulence intensity in wind turbine wakes at Middelgrunden offshore wind farm. Wind Energy. 2007;10:517–28. DOI: 10.1002/we.238.
10. Nybø A, Nielsen FG, Reuder J, Churchfield MJ, Godvik M. Evaluation of different wind fields for the investigation of the dynamic response of offshore wind turbines. Wind Energy. 2020;23:1810–28. DOI: 10.1002/we.2518.
11. Churchfield MJ, Lee S, Michalakes J, Moriarty PJ. A numerical study of the effects of atmospheric and wake turbulence on wind turbine dynamics. J Turbul. 2012;13:N14. DOI: 10.1080/14685248.2012.668191.
12. Liao D, Zhu SP, Correia JAF, De Jesus AMP, Veljkovic M, Berto F. Fatigue reliability of wind turbines: Historical perspectives, recent developments and future prospects. Renew Energy. 2022;200:724–42. DOI: 10.1016/j.renene.2022.09.093.
13. Katsaprakakis DA, Papadakis N, Ntintakis I. A comprehensive analysis of wind turbine blade damage. Energies. 2021;14:5974. DOI: 10.3390/en14185974.
14. Asim T, Islam SZ. Effects of damaged rotor on wake dynamics of vertical axis wind turbines. Energies. 2021;14:7060. DOI: 10.3390/en14217060.
15. Chatelain P, Duponcheel M, Zeoli S, Buffin S, Caprace DG, Winckelmans G, et al. Investigation of the effect of inflow turbulence on vertical axis wind turbine wakes. J Phys Conf Ser. 2017;854. DOI: 10.1088/1742-6596/854/1/012011.
16. Armenta-Déu C. Improved marine wind farm layout. J Offshore Struct Technol. 2023;10:12–22.
17. Armenta-Déu C, Piqueras D. Performance of drag FOWT under variable pitch. Innovation and lecture notes on novel advances for renewable energy systems. The 4th Workshop on Wind and Marine Energy (WWME). Universidad del País Vasco; 2023. p. 35–8. ISBN: 978-84-1319-526-1.
18. Tandel R, Shah S, Tripathi S. A state-of-art review on bladeless wind turbine. J Phys Conf Ser. 2021;1950. DOI: 10.1088/1742-6596/1950/1/012058.
19. Adeyanju AA, Boucher D. Theoretical analysis of the bladeless wind turbine performance. J Sci Res Rep. 2020;26:93–106. DOI: 10.9734/jsrr/2020/v26i1030325.
20. Francis S, Umesh V, Shivakumar S. Design and analysis of vortex bladeless wind turbine. Mater Today Proc. 2021;47:5584–8. DOI: 10.1016/j.matpr.2021.03.469.

21. Predin A, Fike M, Pezdevšek M, Hren G. Alternative wind energy turbines. In: Peddapelli SK, Virtic P, editors. Wind and Solar Energy Applications: Technological Challenges and Advances. Boca Raton (FL): CRC Press; 2023. p. 323–32. DOI: 10.1201/9781003321897-24.
22. Badri N, Peddolla V, Gottumukkala H, Jyothi US, S A. Design and analysis of bladeless wind turbine. In: E3S Web Conf. EDP Sci. 2023;391. DOI: 10.1051/e3sconf/202339101040.
23. Shanbough GR, Nirmalraj AA, George THP. Design of A bladeless wind turbine. Int J Sci Eng Technol Res. 2015;4:710–4.
24. Das A, Azimi N. CFD modeling of the movement of bladeless wind turbines. Iran J Chem Eng. 2024;20:40–55.
25. Thomai MP, Kharsati L, Rama Samy N, Sivamani S, Venkatesan H. Experimental analysis of vortex induced vibration in the bladeless small wind turbine. In: Proceedings of the ASME 2019 Gas Turbine India Conference. Vol. 2: Combustion, Fuels, and Emissions; Renewable Energy: Solar and Wind; Inlets and Exhausts; Emerging Technologies: Hybrid Electric Propulsion and Alternate Power Generation; GT Operation and Maintenance; Materials and Manufacturing (Including Coatings, Composites, CMCs, Additive Manufacturing); Analytics and Digital Solutions for Gas Turbines/Rotating Machinery. Chennai, Tamil Nadu, India; 2019 Dec 5–6. V002T06A009. ASME. DOI: 10.1115/GTINDIA2019-2484.
26. Chizfahm A, Yazdi EA, Eghtesad M. Dynamic modeling of vortex induced vibration wind turbines. Renew Energy. 2018;121:632–43. DOI: 10.1016/j.renene.2018.01.038.
27. Mate A, Rathod K, Kashiwar V, Patil S, Nimje K, Lawate SV, Kimmatkar KM. Bladeless wind turbine. Int J Res Publ Rev. 2024 May;5(5):9658-9667.
28. Davang S, Manade SK, Patil GS, Patil PS, Bhandari AM. Bladeless wind turbine. Int J Innov Eng Res Technol. 2018 Apr;5(4):36-39.
29. Kumar SA, Prasat MH, Vignesh R, Rao DDK, Vijay A, Elizabeth SRC, Stanley MJ. Design, fabrication, and analysis of bladeless turbine. In: IOP Conf Ser. Mater Sci Eng. 2020;993(1):012158.
30. Badri N, Peddolla V, Gottumukkala H, Jyothi US, S A. Design and analysis of bladeless wind turbine. In: E3S Web Conf. EDP Sci. 2023;391. DOI: 10.1051/e3sconf/202339101040.
31. Armenta-Déu C, Madrazo I, Contreras J, Santos M. Vibrational wind turbine design. J Offshore Struct Technol. 2024.
32. Manwell JF, McGowan JG, Rogers AL. Wind Energy Explained: Theory, Design and Application. New York: John Wiley & Sons; 2010.
33. Burton T, Jenkins N, Sharpe D, Bossanyi E. Wind Energy Handbook. John Wiley & Sons; 2011. DOI: 10.1002/9781119992714.
34. Efficiency evolution of a wind turbine with wind speed. Available from: https://qcon-assets-production.s3.amazonaws.com/images/provas/40604/1b.jpg.
35. Thönnißen F, Marnett M, Roidl B, Schröder W. A numerical analysis to evaluate Betz's Law for vertical axis wind turbines. In: J Phys Conf Ser. IOP Publ. 2016;753:022056. DOI: 10.1088/1742-6596/753/2/022056.
36. Tandel R, Shah S, Tripathi S. A state-of-art review on bladeless wind turbine. J Phys Conf Ser. 2021;1950:012058. DOI: 10.1088/1742-6596/1950/1/012058.

